DOI: 10.1002/ejic.200800380

Magnetic Coupling and Anisotropy in a Series of Mixed Chain Charge-Transfer Salts $[M(Cp^*)_2][M'(tds)_2]$ (M = Fe, Mn, Cr; M′ = Ni, Pt)

Sandra Rabaça,[a] Bruno J. C. Vieira,[a] Rui Meira,[a] Isabel C. Santos,[a] Laura C. J. Pereira,[a] M. Teresa Duarte,[b] and Vasco da Gama*[a]

Keywords: Donor–acceptor systems / Metallocenes / Se ligands / Through-space interactions / Magnetic properties / Magnetic anisotropy

The preparation of new charge-transfer (CT) salts based on the decamethylmetallocenium donors (D), $[M(Cp^*)_2]$ (M = Mn, Cr), and on the bis[bis(trifluoromethyl)ethylene diselenolato]metalate(III) acceptors (A), $[M'(tds)_2]$ (M = Ni, Pt), yielded four new members of the family of CT salts $[M(Cp^*)_2][M'(tds)_2]$ {M/M′ = Fe/Ni (**1**), Fe/Pt (**2**), Mn/Ni (**3**), Mn/Pt (**4**), Cr/Ni (**5**), Cr/Pt (**6**)}. Their crystal structures consist of an arrangement of parallel mixed chains, DADADA, with short D–A contacts and large interchain separations. The CT salts **1**–**5** are isostructural and **6** shows minor differences in the interchain arrangements. The analysis of the intermolecular contacts, in the framework of the McConnell I model, provides a fair interpretation of the magnetic coupling. The behavior of these salts is dominated by the ferromagnetic (FM) D–A intrachain interactions. Coexisting weaker antiferromagnetic (AF) interchain couplings induce AF transitions in **2**, **3**, **4**, and **6**, with T_N = 3.3, 2.1, 5.8, and 5.2 K, respectively. The intrachain coupling and the T_N values of the CT salts based on the $[M(Cp^*)_2]$ (M = Fe, Mn) donors (**1**, **2**, **3**, and **4**) were found to be in good agreement with those predicted by the mean field model. Compounds **5** and **6** exhibit weaker intrachain coupling and lower critical temperatures than those predicted by that model, which is attributed to weaker D–A interactions. The study of the low temperature behavior of the salts **3**, **4**, and **6** allowed the disclosure of the effect of the magnetic anisotropy of the donors. The CT salts based on highly anisotropic donors, such as **3** and **4**, show metamagnetic (MM) behavior, with phase diagrams that include a paramagnetic (PM) and an AF phase, as previously observed for **2**. In the phase diagram of **6**, where the $[Cr(Cp^*)_2]$ donor does not show magnetic anisotropy, a spin-flop (SF) phase is present in addition to the PM and AF phases. This is the first time an SF phase was observed in $[M(Cp^*)_2]$-based CT salts.
(© Wiley-VCH Verlag GmbH & Co. KGaA, 69451 Weinheim, Germany, 2008)

Introduction

Following theoretical strategies developed in the 1960s[1] to obtain intermolecular ferromagnetic (FM) coupling in molecule-based materials, the synthesis and study of charge-transfer (CT) salts based on decamethylmetallocene donors and on planar acceptors has proven to be a quite successful approach, in the last three decades, in the search of new molecular materials exhibiting magnetic cooperative phenomena. The combination of these donors with acceptors such as olefin or quinone substituted with electron-withdrawing groups or with metal bis(dichalcogenato) planar, monoanionic complexes allowed the preparation of a large number of CT salts that present a wide variety of phenomena.[2] This approach provided not only isolated examples of magnets but also families of electronically and structurally related compounds, where systematic relationships can be developed.

The crystal structure in these CT salts is typically based on parallel arrangements of mixed chains, where acceptors (A) alternate with donors (D). The basic chain motive seems to be strongly dependent on factors such as the size of the acceptors and on the tendency of the acceptors to form dimers in the solid state.[2b] For small acceptors, the most common basic chain motive is ···DADADA···. For larger acceptors, two types of chain motives are observed, either side-by-side pairs of donors (DD) that alternate with face-to-face pairs of acceptors (AA), ···(DD)AA(DD)AA···, or with isolated acceptors, ···(DD)A(DD)A···. In this class of materials, the intermolecular spin coupling is through-space, and usually these compounds exhibit a large magnetic anisotropy resulting from the coexistence of relatively strong intrachain π–π (D–A or A–A) interactions with weak interchain interactions resulting from the large interchain separations. This anisotropy allows a separate treatment of the intra and interchain magnetic interactions.

[a] Departamento de Química, Instituto Tecnológico e Nuclear/CFMCUL,
Estrada Nacional 10, 2686-953 Sacavém, Portugal
Fax: +351-219941455
E-mail: vascog@itn.pt
[b] Departamento de Engenharia Química, Instituto Superior Técnico,
Av. Rovisco Pais, 1049-001 Lisboa, Portugal
Supporting information for this article is available on the WWW under http://www.eurjic.org or from the author.

 © 2008 Wiley-VCH Verlag GmbH & Co. KGaA, Weinheim

Since magnetic ordering is 3D, the understanding of the mechanism of through-space interactions is one of the most challenging problems in the field.[2a]

In the interpretation of the magnetic intermolecular coupling of this type of materials, two approaches were advanced. The first[3] is based on the McConnell II mechanism,[1b] which involves D–A charge transfer, while the second,[4] based on the McConnell I mechanism,[1a] involves spin-polarization effects. Recent solid-state NMR studies[5] and polarized neutron diffraction experiments[6] seem to be in agreement with the McConnell I mechanism. Even though the validity of this model is still controversial, the McConnell I mechanism has shown remarkable success in the discussion of the intermolecular coupling of this type of materials.

Our group has devoted significant effort in the study of decamethylmetallocenium-based CT salts with metal bis(dichalcogenato) planar acceptors. These acceptors seem to be promising candidates for the synthesis of mixed-stack molecular CT salts with cooperative magnetic phenomena resulting from their planar molecular structures and from the possible extended magnetic interactions mediated by the peripheral chalcogen atoms.[7] In a previous paper, we reported the synthesis and magnetic behavior of the CT salts $[Fe(Cp^*)_2][Ni(tds)_2]$ (**1**) and $[Fe(Cp^*)_2][Pt(tds)_2]$ (**2**).[8] These compounds are isostructural, and their crystal structures consist of a parallel arrangement of ···DADADA··· chains. The magnetic intermolecular couplings in **1** and **2** were analyzed in the framework of the McConnell I mechanism. Furthermore, the relationship between the crystal structure and the magnetic behavior of **1** and **2** and other $[Fe(Cp^*)_2]^+$-based CT salts that exhibit related crystal structures such as $[Fe(Cp^*)_2][Ni(edt)_2]$ (edt = ethylenedithiolato), a metamagnet with T_N = 4.2 K,[9] $[Fe(Cp^*)_2][Ni(tdt)_2]$ [tdt = bis(trifluoromethyl)ethylenedithiolato], a paramagnet down to 1.8 K,[10] and $[Fe(Cp^*)_2][Pt(tdt)_2]$, a paramagnet down to 2 K,[11] were also reported.[8]

In the present work the study of the structure–magnetic-behavior relationship in this family of compounds is extended to the CT salts $[Mn(Cp^*)_2][M'(tds)_2]$, with M′ = Ni (**3**),[12] Pt (**4**), and $[Cr(Cp^*)_2][M'(tds)_2]$, with M′ = Ni (**5**), Pt (**6**) (Scheme 1). The salts **1**–**5** are isostructural, while **6** shows minor differences in the interchain arrangements. The $[M(Cp^*)_2]^+$ (M = Mn and Cr) donors are expected to provide valuable insight into the effect of varying the spin value and magnetic anisotropy of the donors on the magnetic behavior of this family of compounds. Likewise in the strongly anisotropic S = 1/2 $[Fe(Cp^*)_2]^+$ donor ($g_\parallel$ = 4.4, $g_\perp$ = 1.3, and $\langle g \rangle$ = 2.8[3]), the dispersion of the g values (deduced from measurements in polycrystalline powder samples), ranging from 2.2 to 2.9[13] in the S = 1 $[Mn(Cp^*)_2]^+$ donor, also suggests considerable magnetic anisotropy. In contrast, the S = 3/2 $[Cr(Cp^*)_2]^+$ donor does not show any magnetic anisotropy ($g_\parallel$ = 2.0, $g_\perp$ = 2.0[14]).

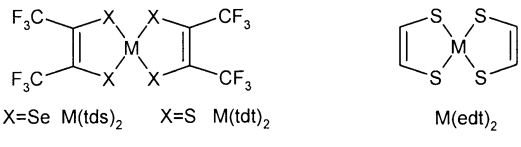

Scheme 1. Molecular structure of the $[M(tds)_2]^-$, $[M(tdt)_2]^-$, and $[M(edt)_2]^-$ acceptors.

In order to further contribute to the investigation of the salts that exhibit magnetic ordering at low temperatures, we have undertaken a detailed study using dc magnetization and ac susceptibility measurements.

Results and Discussion

Synthesis

CT salts **3**–**6** were obtained by the addition of concentrated acetonitrile solutions of the decamethylmetallocenium salts $[Mn(Cp^*)_2]PF_6$[13d] or $[Cr(Cp^*)_2]PF_6$[14] in stoichiometric amounts to concentrated methanol solutions of nBu$_4$N$[Ni(tds)_2]$[15] or nBu$_4$N$[Pt(tds)_2]$.[15] After concentration, crystalline precipitates were collected by vacuum filtration. Dark needle-shaped single crystals suitable for X-ray diffraction were obtained by slow evaporation of the concentrated solutions of compounds **3**–**6** (see details in the Experimental Section).

Crystal Structures

Compounds **3**–**5** are isostructural and crystallize in the triclinic system, while **6** crystallizes in the monoclinic system. In the asymmetric unit of compounds **3**–**6**, there is one independent half-anion and one independent half-cation units, where the metal atoms are located at inversion centers. The details of the crystal structure determination of CT salts **3**–**6** are presented in the Experimental Section. The $[M(Cp^*)_2]^+$ donors show a C_5 local symmetry, and the two Cp rings present a staggered conformation. The $[M'(tds)_2]^-$ acceptors are planar and have a D_{2h} local symmetry. The bond lengths and angles of the donors and acceptors are in the expected ranges. Molecular graphics were prepared with SCHAKAL-97.[16]

The CT salts **3**–**5** are isostructural with the $[Fe(Cp^*)_2]^+$ analogues (**1** and **2**),[8] and, although **6** exhibits a distinct crystal structure, all these CT salts present similar supramolecular arrangements. Their crystal structures consist of an arrangement of parallel 1D chains with alternating donors (D) and acceptors (A), ···DADADA···, similar to that observed in other decamethylmetallocenium CT salts, in particular in the salts with small metal–bis(dichalcogenato) acceptors.[2b] Compounds **1**–**5** present similar interchain arrangements, while in **6**, a slightly distinct arrangement is observed, as shown in Figure 1. In the case of **1**–**5**, the stacking axis corresponds to [001], and in **6**, to [100]. The interchain arrangements are shown in Figure 1a and b (CT salts **4** and **6**) and in Figure 2 (**4**).

Within the chains, the donors and acceptors are slightly tilted relative to the stacking axis (by ca. 8–9°), and the acceptors molecules are nearly parallel to the Cp rings of the donors. The metallic element (M′ = Ni or Pt) from the

 © 2008 Wiley-VCH Verlag GmbH & Co. KGaA, Weinheim

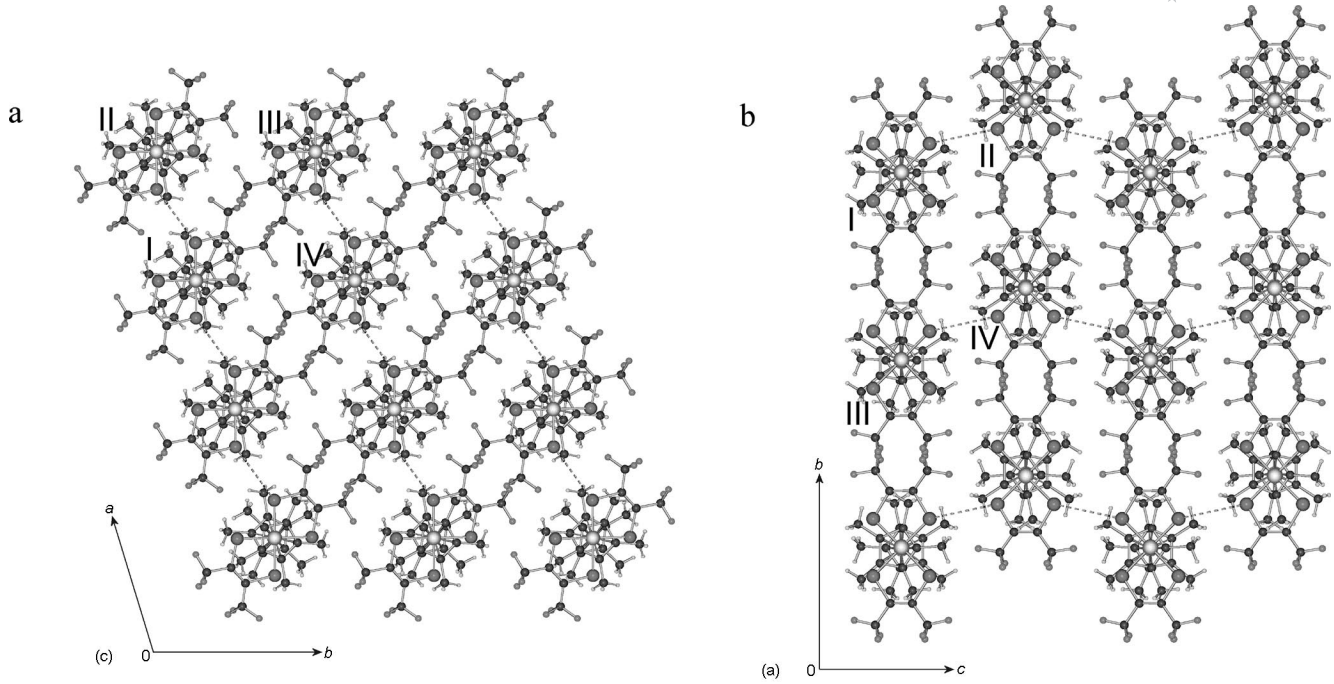

Figure 1. (a) View of the crystal structure of **4** along the stacking axis [001], (b) view of the crystal structure of **6** along the stacking axis [100]. The short dashed lines show the shorter Se–Se interchain contacts.

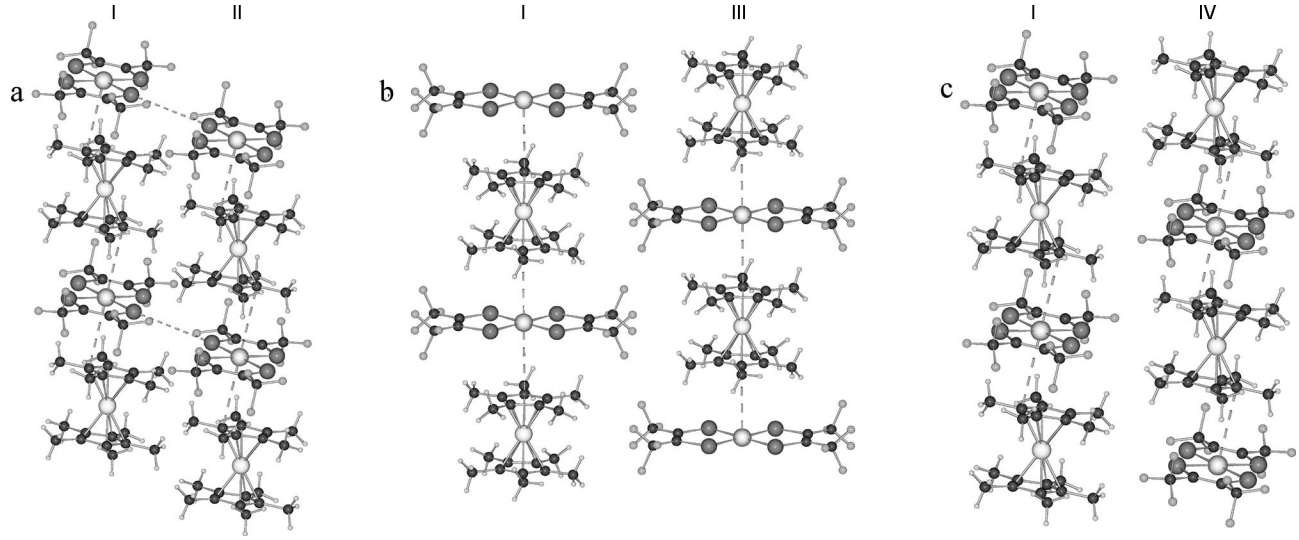

Figure 2. (a) View of the interchain arrangement in the I–II pair in compound **4** [the long dashed lines represent the shorter intrachain D–A contacts (Pt–C) and the short dashed lines the shorter interchain Se–Se contacts]; (b) view of the interchain arrangement in the pair I–III; (c) view of the interchain arrangement in the pair I–IV.

acceptors is above the Cp ring and is slightly shifted off center. Relatively short intrachain D–A contacts are observed in these salts, which involve Ni or Pt and Se atoms from the acceptors and C atoms of the Cp rings from the donors. In particular, in the $[Pt(tds)_2]^-$-based compounds (**2**, **4**, and **6**), there are contacts with separations (d) that are closer than the sum of the van der Waals radii (d_W),[16] $q = d/d_W = 0.98$, 0.98 and 0.97, for **2**, **4**, and **6**, respectively. In the $[Ni(tds)_2]^-$-based salts, those separations are slightly larger, $q = 1.04$, 1.02 and 1.03, for **1**, **3**, and **5**, respectively. Details of the intrachain arrangements of the CT salts **1**–**6** are presented as Supporting Information.

A view normal to the chains is shown in Figure 1a and b for compounds **4** and **6**, respectively. It is possible to notice the distinct interchain arrangement in the case of **6**, where the interchain Se···Se contacts present a zig-zag conformation along c, while in compounds **1**–**5**, the Se···Se contacts present a regular arrangement roughly along a. In the

 © 2008 Wiley-VCH Verlag GmbH & Co. KGaA, Weinheim

Table 1. Summary of the interchain distances and selected interchain interatomic separations in compounds **1**–**6**.

	1[a]	**2**[a]	**3**	**4**	**5**	**6**
$d^{I–II}$ (Å)[b]	8.338	8.388	8.342	8.403	8.352	8.382
$d^{I–III}$ (Å)[b]	10.898	11.002	10.875	10.983	10.859	10.842
$d^{I–IV}$ (Å)[b]	9.953	9.958	9.936	9.957	9.935	9.868
$c^{I–II}$ (Å), q[c]	4.582, 1.15	4.349, 1.09	4.574, 1.14	4.331, 1.08	4.568, 1.14	4.234, 1.06

[a] Ref.[8] [b] Interchain distance. [c] Shorter Se–Se contact in neighboring chains (pair I–II).

crystal structures of these CT salts, each chain has six neighboring chains, but only three unique interchain arrangements are observed (I–II, I–III and I–IV), as illustrated in Figure 2 for compound **4**. Besides a few short contacts involving H atoms (mainly F···H), short A–A interchain separations are also observed, which involve Se atoms in the I–II pairs of chains. The above-mentioned M′···C intrachain contacts are represented in Figure 2 by dashed lines, and the Se···Se interchain contacts are represented in Figure 1 and Figure 2 by the shorter dashed lines.

As shown in Figure 2 for compound **4**, the chains in the I–II pairs are essentially in-registry (AA and/or DD closer interchain separations), while I–IV and I–III are out-of-registry (DA closer interchain separations). The closest interchain separation is found in the pair I–II, while the largest separation corresponds to the pair I–III. In spite of the distinct disposition of the chains (Figure 1), a similar interchain arrangement is observed in **6**. The interchain separations ($d^{I–II}$, $d^{I–III}$, and $d^{I–IV}$) and the closest Se–Se distances ($c^{I–II}$) are summarized in Table 1, a more detailed description of the interchain arrangements is presented as Supporting Information. Even though the interchain distances are slightly longer in the salts based on the $[Pt(tds)_2]^-$ acceptor (**2**, **4**, and **6**) than in those based on the $[Ni(tds)_2]^-$ acceptor (**1**, **3**, and **5**), the Se···Se interchain contacts ($c^{I–II}$) for the CT salts **2**, **4**, and **6** are considerably shorter than those in compounds **1**, **3**, and **5**.

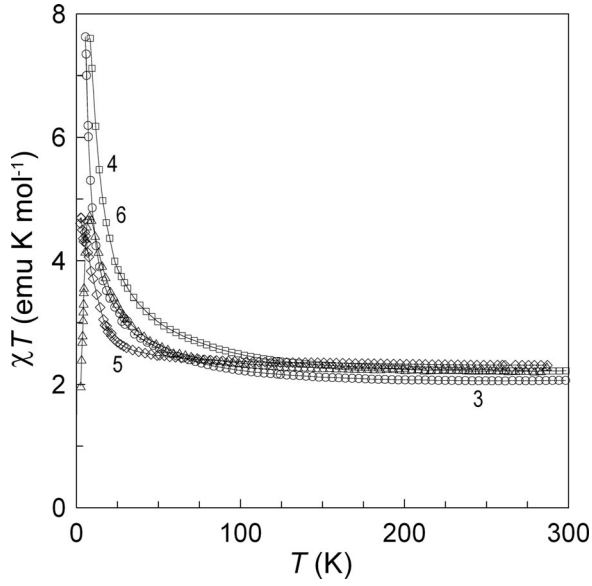

Figure 3. Temperature dependence of χT for compounds **3** (○), **4** (□), **5** (✧), and **6** (Δ).

Table 2. Weiss constants (θ), experimental and calculated effective magnetic moments and Néel temperature of the CT salts **1**–**6**.

	1[a]	**2**[a]	**3**[b]	**4**[b]	**5**[b]	**6**[b]
θ (K)	8.9	9.3	12.8	16.6	2.3	9.8
μ_{eff}^{RT} (μ_B)	3.01	3.35	4.07	4.21	4.30	4.21
$\mu_{eff}^{calcd.}$ (μ_B)	3.01	3.01	3.57	3.57	4.26	4.26
T_N (K)	—[c]	3.3	2.1	5.8	—[c]	5.2

[a] Ref.[8] [b] This work. [c] no magnetic ordering was observed.

Magnetic Properties

Magnetic Coupling

The temperature dependence of the magnetic susceptibility of compounds **3**–**6** was obtained in the temperature range 1.7–300 K, with polycrystalline samples. Figure 3 shows the temperature dependence of χT for the CT salts **3**–**6**. Above 30 K, the molar magnetic susceptibilities (χ) of the salts could be fitted to the Curie–Weiss law [$\chi = C/(T - \theta)$] with positive θ values (Table 2) similarly to previous results for **1** and **2**. This is a clear indication of the existence of dominant FM interactions in this family of compounds. A summary of the magnetic parameters obtained for compounds **1**–**6** is listed in Table 2.

For the $[Mn(Cp^*)_2]^+$-based compounds, **3** and **4**, the room-temperature effective magnetic moments (μ_{eff}^{RT}) are higher than the calculated values ($\mu_{eff}^{calcd.}$), where the average g value of the donor ($<g_D>$) was taken as 2.2, which corresponds to the lowest value reported in the literature.[13d] This difference is attributed to orientation effects due to the applied field and the large anisotropy of the g values of the donor. The obtained g values for the donors (g_D) in these two compounds are 2.58 and 2.70 for **3** and **4**, respectively. In the case of the $[Cr(Cp^*)_2]^+$-based compounds **5** and **6**, where $g_{\|} = g_{\perp} = <g_D> = 2$,[14] a good agreement was obtained between the experimental and calculated values of μ_{eff}. As previously reported for $[Fe(Cp^*)_2]^+$-based compound **2**,[8] the large anisotropy of this donor is responsible for the high values obtained for μ_{eff}^{RT}. With compound **1**, the good agreement between the experimental and calculated μ_{eff} values is attributed to a different sample preparation, where a compressed pellet was used to prevent the orientation effects arising from the applied magnetic field.

The magnetic behavior exhibited by this family of compounds clearly suggests the coexistence of strong intrachain FM interactions with weaker antiferromagnetic (AF) in-

 © 2008 Wiley-VCH Verlag GmbH & Co. KGaA, Weinheim

terchain interactions. As previously reported for compound **2**, a metamagnet with T_N = 3.3 K[8] at low temperatures and low applied magnetic fields, the presence of AF transitions were also observed for compounds **3**, **4**, and **6**. Furthermore, these compounds were also observed to exhibit field-induced transitions when high enough magnetic fields are applied. A detailed study of the low-temperature magnetic behavior of compounds **3**, **4**, and **6** will be presented.

According to a simple mean-field model, where it is assumed that the intra- and interchain interactions remain unchanged as the donor is varied, T_c can be calculated for different values of S_D or S_A.[17] By scaling T_c, as $T_c^* = T_c(S_D)/T_c(S = 1/2)$, values of T_c^* = 1, 1.7, and 2.5 for S_D = 1/2, 1, and 3/2, respectively, were obtained. Given the simplicity of the model, a good relationship has been found for the observed T_c values of systems with S_D = 1/2 and 1 {i.e. with CT salts based on the donors $[M(Cp^*)_2]^+$, M = Fe and Mn}. This relationship, however, seems to fail systematically with the S = 3/2 $[Cr(Cp^*)_2]^+$ salts, where a T_c value that is 1/3 to 1/2 of the predicted value is frequently obtained. The failure in case of the $[Cr(Cp^*)_2]^+$ salts can be due to lower J values for those salts. A reasonable agreement with the mean-field predictions for the relation between the T_N values of **2** and **4** is obtained with T_N(**4**)/T_N(**2**) = 1.76. A T_N value of 1.2 K is estimated for **1** by considering that T_N = 2.1 K for **3**.

Relationship between Crystal Structure and Magnetic Behavior

In order to discuss the nature of the magnetic interactions in this family of compounds, a qualitative comparative analysis based on the McConnell-I mechanism[1a] was performed. In the most common use of this mechanism, the nature of the magnetic intermolecular coupling is determined by the spin density (ρ^S) signs of the atoms involved in the shortest intermolecular contacts between the two interacting radicals. An AF coupling is predicted in the case when both atoms present the same sign for ρ^S, or a FM coupling is predicted if the signs are different.

In agreement with NMR[18] and neutron diffraction[19] studies, atomic ρ^S calculations[8] of the $[Fe(Cp^*)_2]^+$ donor showed that most of the ρ^S resides on the Fe atom (ρ^S_{Fe} = 1.26), and a spin-polarization effect was observed in the C_5Me_5 ligands, where the carbon atoms from the Cp ring have a negative value for ρ^S (ρ^S_C = –0.03) and the C atoms from the methyl groups (C′) show a small positive ρ^S value ($\rho^S_{C'}$ = 0.002). The ρ^S for the methyl H atoms is negligible, ($|\rho^S_H| < 0.002$). A similar spin distribution is expected for the $[M(Cp^*)_2]^+$ (M = Mn and Cr) donors.[18,19] In the case of the acceptors $[M(tds)_2]^-$ (M = Ni, Pt), the ρ^S calculations[8] revealed that most of the ρ^S (> 95%) is located on the central MSe_4 fragment of the acceptors and a residual value (<5%) was found on the ethylene C atoms. The ρ^S was found to be negligible for the atoms from the CF_3 groups ($|\rho^S| < 0.003$).

In a rough evaluation of the intermolecular magnetic coupling of these CT salts, two main factors were considered: (1) the interatomic separations, calculated through the parameter $q = d/d_W$. This value seems to be better for the estimation of the effective interatomic overlap than simply the interatomic separation, d; and (2) the sign and magnitude of ρ^S of the atoms involved in the contacts.

The FM coupling observed in this family of compounds can be ascribed to D–A intrachain interactions. Within the mixed chain, a good overlap between the acceptors and the Cp* ligands is observed with short D–A separations between the Cp rings, in which the C atoms carry a negative ρ^S value of –0.03 (ρ^S = –0.15 for each Cp ring) and the MX_4 central fragment carries a positive ρ^S value (total ≈ 0.95). This is expected to lead to significant FM D–A coupling. The presence of other relatively short contacts (mostly interchain) can be ignored, as they involve atoms that present negligible values for ρ^S, such as H and F, which leads to very weak interactions. In a first approximation, by assuming that the D–A exchange coupling (J_{DA}) is essentially determined by the D–A overlap and that J_{DA} must increase with a decrease in the intermolecular separations and by considering the q values of the M′–C D–A contacts, in this series, J_{DA} should increase in the order **1** ≈ **5** ≈ **3** < **2** ≈ **4** ≈ **6**.

Although the obtained θ values for this series of compounds (Table 2) should be an average of all the intermolecular interactions, these values are expected to essentially be determined by the strong D–A FM intrachain interactions. In this sense, it seems reasonable to admit that the θ values can be used in order to compare the intrachain D–A magnetic coupling in these compounds. In these mixed chain CT salts, the relationship $E_{intra} \propto S_D S_A J_{DA}$ holds[13f] (E_{intra} is the intrachain interaction energy), and for each donor, a good correlation is observed between the θ values and the above-mentioned predicted J_{DA} order. In the case of the CT salts based on the S = 1/2 $[Fe(Cp^*)_2]^+$ donor, θ for **2** is larger than that for **1**, in agreement with a smaller q value of the M′–C contact for compound **2**. A similar relationship is also observed for the CT salts based on the donors S = 1 $[Mn(Cp^*)_2]^+$ (**3** and **4**) and S = 3/2 $[Cr(Cp^*)_2]^+$ (**5** and **6**), where the larger value of θ obtained in **4** and **6** corresponds to closer M′–C contacts.

At low temperatures, AF transitions were observed in the CT salts **2**, **3**, **4**, and **6**, in spite of the fact that the strongest intermolecular interactions are FM (D–A intrachain coupling). Hence, the much weaker AF interchain coupling seems to play a crucial role in this magnetic ordering. The stronger interchain interactions must be related to the relatively short Se···Se contacts, which involve acceptors located in neighboring chains (I–II pairs of chains). These contacts are expected to lead to sizeable AF interactions, as the Se atoms carry significant ρ^S (≈ 0.2).

In this family of compounds, the separation between acceptors in the pair of chains I–II suggests that the AF A–A coupling must increase in the order **1** ≈ **3** ≈ **5** < **2** ≈ **4** ≈ **6**. In this case, it is expected that $T_N \propto |E_{intra}E_{inter}|^{1/2}$,[13f] where E_{inter} is the effective interchain interaction energy. The considerably smaller T_N value for **3** (T_N = 2.1 K) than that for compound **4** (T_N = 5.8 K) and the absence of AF

 © 2008 Wiley-VCH Verlag GmbH & Co. KGaA, Weinheim

ordering in the salts **1** and **5** down to 1.6 K must be related to weaker inter- and/or intrachain coupling. However, these compounds are expected to exhibit AF ordering at lower temperatures ($T_N < 1.6$ K).

Low-Temperature Magnetic Behavior

The phase diagrams of antiferromagnets can be classified into two classes, where each class exhibits a distinct $H(T)$ behavior upon application of a magnetic field parallel to their axis of antiparallel alignment.[20] Class 1 antiferromagnets are highly anisotropic with a field-induced first-order phase transition ($T < T_N$) arising from the reversal of the local spin directions. This process is called a metamagnetic (MM) phase transition, and compounds belonging to Class 1 antiferromagnets are called metamagnets. It is worth mentioning that this MM transition is first order between T = 0 K up to the tricritical temperature (T_T) ($0 < T_T < T_N$) and is second order between T_T and T_N. In contrast, Class 2 antiferromagnets exhibit weak or even no magnetic anisotropies. In the typical magnetic phase diagram, besides the AF and paramagnetic (PM) regions, an extra phase, classified as the spin-flop (SF) region is present, which separates the AF and PM phases at low temperatures. In this class of antiferromagnets, the application of a sufficiently high magnetic field induces a first-order phase transition, associated with the flopping of the spins such that they are aligned perpendicular to the applied field. In the SF region, the applied field induces a rotation of the spins from antiparallel to a parallel orientation.

In the series **1**–**6**, compounds based on the highly anisotropic $[M(Cp^*)_2]^+$ (M = Fe and Mn) donors (**1**–**4**) are expected to behave as Class 1 antiferromagnets, while compounds **5** and **6** are expected to behave as Class 2 antiferromagnets, since the $[Cr(Cp^*)_2]^+$ donor does not exhibit magnetic anisotropy. The phase diagram previously reported for **2**[8] is consistent with that expected for a Class 1 antiferromagnet. A detailed analysis of the magnetic behavior at low temperatures for compounds **3**, **4**, and **6**, which exhibit AF transitions, is presented below.

[Mn(Cp)$_2$][Ni(tds)$_2$] (**3**)*

The temperature dependence of the field-cooled (FC) magnetic susceptibility $\chi(T)$ of compound **3** with applied magnetic fields of 2, 40, 400, and 500 G is shown in Figure 4a. The maxima observed at low fields indicate the existence of an AF transition at T_N = 2.1 K. With applied fields higher than 400 G, the maximum is no longer detected at temperatures down to 1.8 K. Below T_N, the magnetization isotherms shown in Figure 4b present a clear sigmoidal behavior, which indicates the existence of a field-induced transition. At 1.6 K, for low applied fields, the magnetization increases slowly with H, as for an antiferromagnet; at ca 500 G, the magnetization increases drastically, and at 1.5 kG, it is nearly saturated. At this temperature (1.6 K), the critical field (H_c), defined as the maximum in dM/dH, is ≈ 500 G. The phase diagram for compound **3**, obtained from the dc magnetization measurements, is shown in the inset of Figure 4b. The strong magnetic anisotropy of the donor and the field-dependent behavior are consistent with a MM transition, similar to that observed in **2**,[8] with T_N = 3.3 K and H_c = 3.95 kG at 1.7 K.

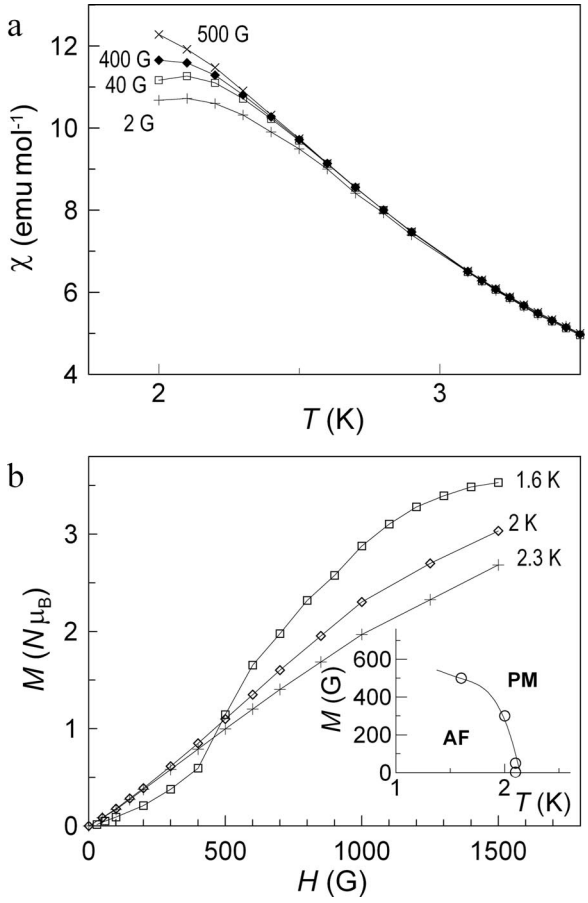

Figure 4. (a) Temperature dependence of χ for compound **3**, obtained at 2 (+), 40 (□), 400 (♦), and 500 G (×); (b) magnetization isothermal curves of **3**, obtained at 1.6 (□), 2 (✧), and 2.3 K (+). The phase diagram of **3** is shown in the inset of (b).

[Mn(Cp)$_2$][Pt(tds)$_2$] (**4**)*

As previously described for compounds **2**[8] and **3**, the isofield and isothermal dc magnetization curves obtained for compound **4** are also consistent the existence of a MM behavior (Figure 5). In this case, however, the AF phase transition occurs at a significantly higher temperature, T_N = 5.8 K. Furthermore, for $T \leq 3.2$ K, the field-induced transitions are quite sharp and begin to exhibit hysteresis (increasing upon cooling). This can easily be seen in the 1.6 K isothermal, where both the measurements with increasing (closed squares; solid line) and decreasing (open squares; dashed line) applied fields are shown. This behavior indicates that below 3.2 K the field-induced transition is a first-order phase transition, with $3.2 \leq T_T \leq 4$ K. At 1.6 K, $H_c \approx 3.9$ kG is an average obtained from the maxima of dM/dH of the isothermal curves (with increasing and decreasing fields).

The temperature dependence of the real and imaginary components of the ac susceptibility [$\chi'(T)$ and $\chi''(T)$] at fixed dc fields (from 0 to 6 kG) is shown in Figure 6. With

 © 2008 Wiley-VCH Verlag GmbH & Co. KGaA, Weinheim

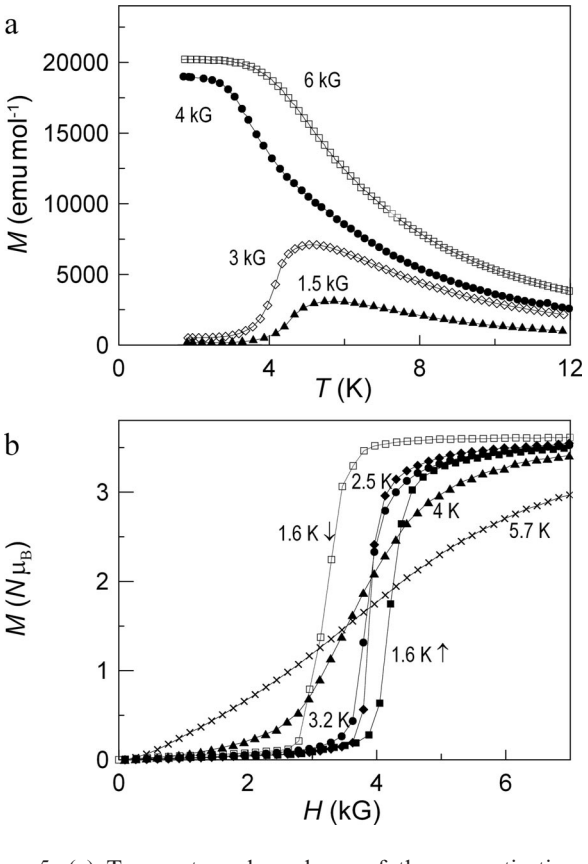

Figure 5. (a) Temperature dependence of the magnetization for compound **4**, obtained at 1.5 (▲), 3 (△), 4 (●),and 6 kG (□); (b) magnetization isothermal curves of **4**, obtained at 1.6 ($H\uparrow$ ■; $H\downarrow$ □), 2.5 (♦), 3.2 (●), 4 (▲), and 5.7 K (×).

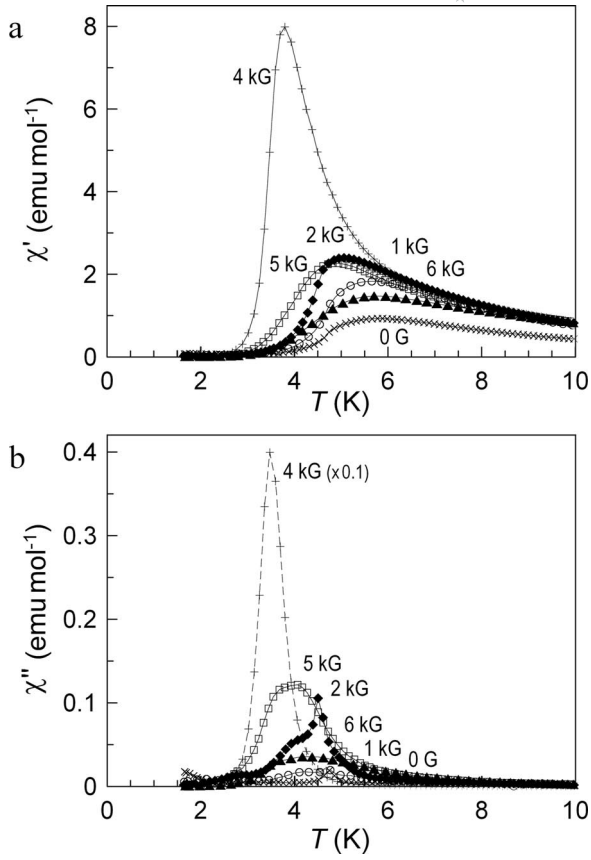

Figure 6. (a) Temperature dependence of χ' for compound **4**, obtained at 0 (×), 1 (○), 2 (♦), 4 (+), 5 (□), and 6 kG (▲); (b) temperature dependence of χ'' for **4**.

a applied dc magnetic field of 0 G and with an ac field of 1 G, a frequency independent peak at T_N is detected in the real component of the ac susceptibility, χ', as expected for an antiferromagnet. Just below T_N, a weak sign is detected in the imaginary component, χ'', which is probably due to the existence of a weak residual magnetic field. With increasing applied fields of up to 4 kG, the intensity of the χ' peak increases and the maxima shifts to lower temperatures (Figure 6a). For $H > 4$kG, the peaks tend to broaden, their intensity decreases, and they shift to higher temperatures. As shown in Figure 6b, a similar behavior is observed for $\chi''(T)$.

The applied magnetic-field dependence of the ac susceptibility, $\chi'(H)$ and $\chi''(H)$, at fixed temperatures (from 1.6 to 5.7 K) is shown in Figure 7. At temperatures lower than 3 K, $\chi'(H)$ shows a very weak signal, with a broad peak at ≈ 4 kG and a tail at low fields ($H < 2$ kG). However, at higher applied fields, the intensity of the peak at ≈ 4 kG suddenly increases and reaches a maximum at ca. 4 K. With increasing temperature, the $\chi'(H)$ peak then broadens, becomes less intense, and shifts slightly to lower fields. The behavior of $\chi''(H)$ is somewhat similar, although in this case, the intensity maximum is at 3.2 K. The $\chi''(H)$ curves obtained at low temperatures ($T < 3$ K) and at 4.5 K present two relatively broad maxima, one occurs at the same field as the peak observed in $\chi'(H)$ and an additional peak appears at lower fields. At higher temperatures, this signal is so weak that it is hardly detected.

Without going into an in-depth analysis of the field dependence of the ac susceptibility, we would like to comment on the low intensity of the signal below 3.2 K (first-order transition). As a result of the internal field,[21] at low temperatures, $T < T_T$, two peaks are expected to occur for $\chi'(H)$, which correspond to the transition fields H_- and H_+. As the temperature increases, these two fields become equal at $T = T_T$, and for $T_T \leq T \leq T_N$ the transition is second order. The merging of the two transition fields (at $H = H_- = H_+$) can also account for the high intensity of the peaks at 3.2 and 4 K, which indicates that T_T is in the range 3.2–4 K, as suggested by the dc magnetization results. We will assume that $T_T = 3.5 \pm 0.2$ K.

A phase diagram, $H(T)$, of compound **4** is shown in Figure 8. This diagram was obtained from both dc magnetization [$M(T)$ and $M(H)$] and ac susceptibility [$\chi'(T)$ and $\chi'(H)$] results. $H(T)$ includes two distinct magnetic phases, an AF and a PM phase. Within the PM phase, at high fields and low temperatures an FM-like region ("FM") is also defined and corresponds to the high-field state induced by the applied magnetic field. However, there is no evidence that this region corresponds to a real distinct phase. A first-order magnetic phase boundary (I) is present between the AF phase and the "FM" region (dashed line). A second-

 © 2008 Wiley-VCH Verlag GmbH & Co. KGaA, Weinheim

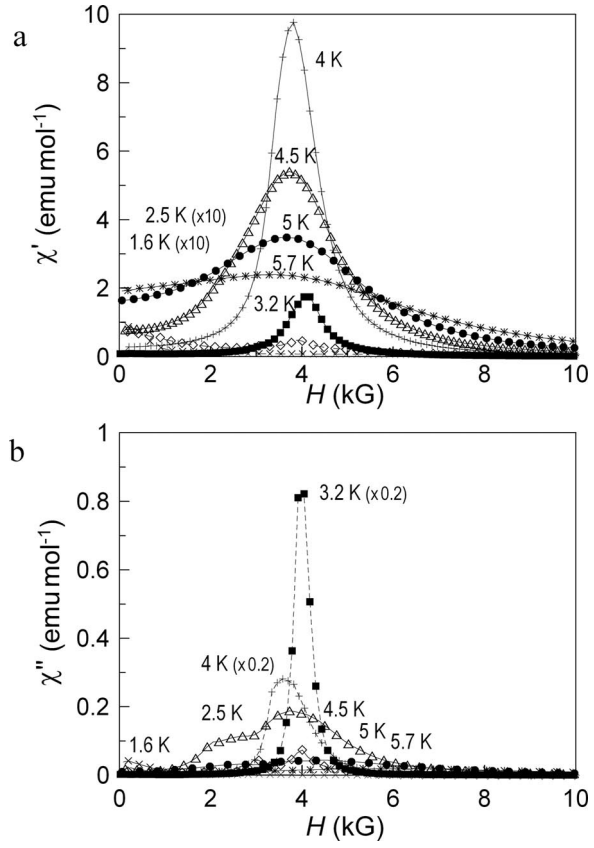

Figure 7. (a) Applied-magnetic-field dependence of χ' for compound **4**, obtained at 1.6 (×), 2.5 (✧), 3.2 (■), 4 (+), 4.5 (Δ), 5 (●), and 5.7 K (∗); (b) applied-magnetic-field dependence of χ'' for **4**.

order phase boundary (II) separates the AF and the PM phases for $T_T < T < T_N$ (solid line). The separation between the "FM" region and the main PM phase is assigned by the dot-dashed line (III). This phase diagram is similar to the one obtained for **2**, apart from the different T_N value. In the case of **2**, it was not possible to detect the first-order phase boundary, because of the lower T_N value for this compound, although the sharpness of the field-induced transitions at $T \leq 2$ K suggests $T_T \approx 2$ K.

It is worth mentioning that, at low temperatures (≈ 1.6 K), similar values for H_c were observed in compounds **4** (H_c = 3.9 kG) and **2** (H_c = 3.95 kG). This is attributed to the similar intrachain AF coupling suggested by structure analysis. This is in good agreement with the results of a simple Ising model that was used in the study of the MM transitions in the compounds $FeCl_2 \cdot 2H_2O$ and $CoCl_2 \cdot 2H_2O$.[22] In these compounds, the H_c values were found to be proportional to the interchain exchange constants. Considerably lower H_c values are anticipated for compounds **1** and **3**, since the interchain coupling is expected to be significantly weaker. While compound **1** does not order above 1.6 K, in the case of compound **3**, it is possible to compare the H_c value at 1.6 K (≈ 500 G) with that obtained for compound **4** at a similar temperature to that of the reduced temperature T/T_N = 1.6/2.1. This would correspond to T = 4.4 K for **4**, where, as predicted, $H_c \approx 3$ kG is considerably higher than in **3**.

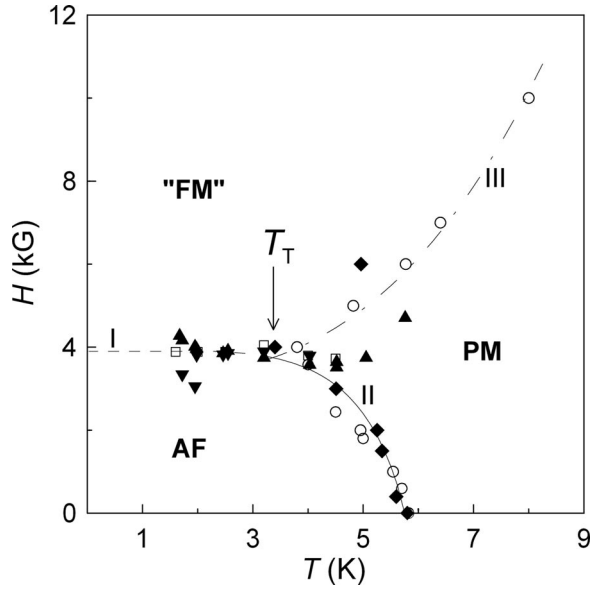

Figure 8. Phase diagram of compound **4**; $M(T)$ (♦), $M(H)$ ($H\uparrow$ ▲, $H\downarrow$ ▼), $\chi'(T)$ (○) $\chi'(H)$ (□); T_T is the tricritical temperature; I denotes the first-order MM transition, II denotes the second-order transition (AF–PM phase boundary), and III denotes the higher-order transitions (from a PM to a FM-like state).

[Cr(Cp)$_2$][Pt(tds)$_2$] (**6**)*

As in compounds **2**, **3**, and **4**, the temperature dependence of the magnetization of **6** (Figure 9a) at low applied magnetic fields shows an AF phase transition with a maximum at ca. 5 K. At low fields, the magnetization decreases with cooling; however, in the $M(T)$ curves with fields of 5 and 10 kG, after the maxima, the magnetization passes through a minimum and increases slightly upon cooling. At 20 kG, this maximum is no longer detected.

In contrast with those observed for compounds **2**, **3**, and **4**, the magnetization isothermal curves of **6** (Figure 9b) reveal the existence of two field-induced transitions; one occurs at ca. 4.9 kG (I) and the second at higher applied magnetic fields (II), as indicated by the applied-field dependence of dM/dH shown in the inset of Figure 9b. In this inset, it is possible to observe two maxima for dM/dH, which correspond to the two field-induced transitions. The transition I is associated with a peak for dM/dH that presents a weak temperature dependence, and at 4 K, this peak is no longer detected, while transition II shows a significant temperature dependence. At 1.6 K, the maximum occurs at ≈ 16 kG, and, as the temperature increases, the maximum shifts considerably to lower fields. Above 3 K, the dM/dH peak broadens significantly. At low temperatures, the dc magnetization behavior clearly suggests the existence of an AF phase at low fields ($H < 4.9$ kG) and an SF phase at higher magnetic fields ($4.9 < H < 16$ kG). As in other materials exhibiting similar behavior,[23] such as α-$MnMoO_4$[23a] and $MnGa_2Se_4$,[23b,23c] a remarkable resemblance is observed in the isothermal magnetization and in the dM/dH field dependence. In particular, the two peaks (I and II) correspond to the AF–SF and SF–PM phase boundaries. Furthermore, a nearly constant behavior for dM/dH is also observed be-

 © 2008 Wiley-VCH Verlag GmbH & Co. KGaA, Weinheim

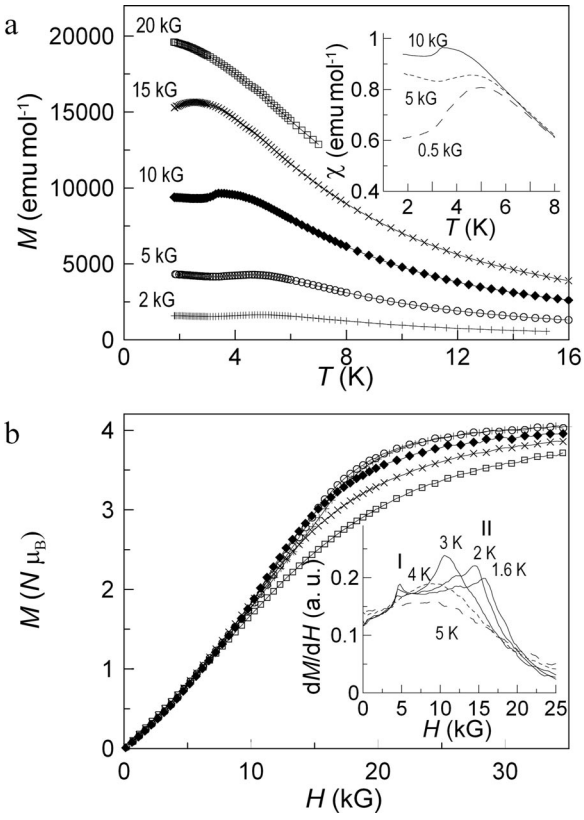

Figure 9. (a) Temperature dependence of magnetization for compound **6**, obtained at 2 (+), 5 (○), 10 (♦), 15 (×), and 20 kG (□). Inset: χ vs. T (with applied fields of 0.5, 5, and 10 kG); (b) magnetization isothermal curves of **4**, obtained at 1.6 (+), 2 (○), 3 (♦), 4 (×), and 5 K (□). Inset: dM/dH vs. H (at the same temperatures).

tween the two maxima. In the case of the magnetization temperature dependence, the $M(T)$ curves crossing the PM–AF ($H < 4.9$ kG) and PM–SF ($H > 4.9$ kG) phase boundaries exhibit a distinct behavior. At low fields, a clear maximum is detected in $M(T)$, while for higher fields ($H >$ 4.9 kG), the magnetization does not show a significant decrease below the peak ($T < T_p$), a behavior that is also observed in α-$MnMoO_4$[23a] and $MnGa_2Se_4$.[23b] This effect can be better seen in the inset of Figure 9a, which shows the temperature dependence of χ at 0.5, 5, and 10 kG.

As expected for an AF transition, at zero dc field, the ac susceptibility of compound **6**, shows a peak in the real component at T_N = 5.2 K and no noticeable signal in the imaginary component. Furthermore, no frequency dependence is observed. The $\chi'(T)$ and $\chi''(T)$ curves, obtained at several applied dc fields (from 0 to 20 kG), are shown in Figure 10. The $\chi'(T)$ behavior is roughly similar to that observed for the static susceptibility, with well-defined peaks below 4.9 kG. However, with slightly larger applied dc fields ($5 < H < 7$ kG), no maxima is observed. In this region, a kink is detected instead, and upon cooling, $\chi'(T)$ continues to increase, but the increase is less pronounced. At higher applied dc fields, the maxima is detected again, but, at low temperatures, $\chi'(T)$ levels out and remains nearly constant. $\chi''(T)$ is practically negligible in the AF phase, where it is maintained within the error of margin of the measurements, and increases slightly in the SF phase, as shown in Figure 10.

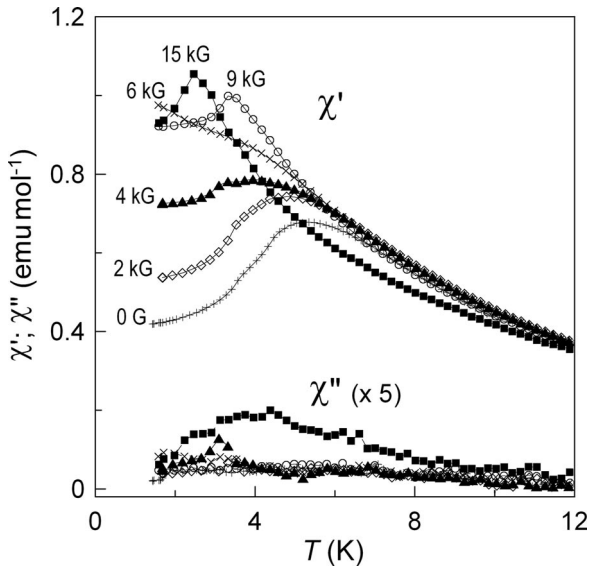

Figure 10. Temperature dependence of χ' and χ'' for compound **6**, obtained at 0 (+), 2 (✧), 4 (▲), 6 (×), 9 (○), and 15 kG (■) (χ'' is multiplied by a factor of 5).

The external dc field dependence of the ac susceptibility, $\chi'(H)$ and $\chi''(H)$, at different temperatures (from 1.6 to 5.2 K) is shown in Figure 11. At low temperatures, two peaks are observed in the curve $\chi'(H)$, which correspond to those observed for dM/dH. Peak I, denoting the SF phase transition, is quite sharp and temperature independent (from 1.65 up to 3 K). At 4 K, a very small shoulder can still be detected, slightly shifted to lower fields. At higher applied dc fields, a second peak is observed, with a similar intensity, but considerably broadened, which corresponds to the SF–PM phase boundary. As in the curve for dM/dH, the peak II position is strongly temperature dependent and shifts to lower fields as the temperature increases. At 4 K, peak II is still observed, but its intensity is considerably reduced and it is considerably broadened. The $\chi''(H)$ curve only shows a sharp peak that seems to be associated with peak I in the $\chi'(H)$ curve. This peak is no longer detected for temperatures ≥4 K. With regard to peak II, no significant contribution could be observed in $\chi''(H)$.

The phase diagram proposed for compound **6** is shown in Figure 12 and was obtained from both dc magnetization data [$M(T)$ and $M(H)$] and the real component of the ac susceptibility [$\chi'(T)$ and $\chi'(H)$] data. This diagram shows three distinct phases, an AF, an SF, and a PM phase. The sharpness of dM/dH and χ' peaks in the field-induced transition I indicates that the SF (AF–SF) transition is first order. While the AF–PM (III) and SF–PM (II) transitions are expected to be second order (phase boundaries represented by the solid line in Figure 12). The first-order SF phase transition (phase boundary corresponds to the dashed line) meets the PM phase boundary at the triple point ($T \approx 3.1$ K, $H \approx 4.9$ kG).

 © 2008 Wiley-VCH Verlag GmbH & Co. KGaA, Weinheim

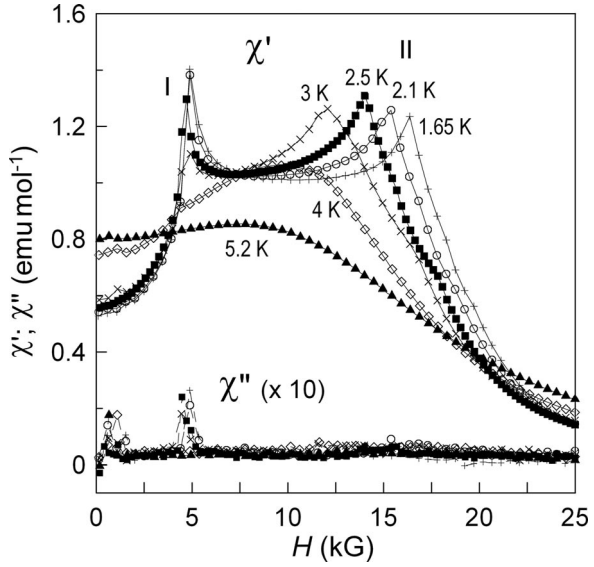

Figure 11. Applied magnetic field dependence of χ' and χ'' for compound **6**, obtained at 1.65 (+), 2.1 (○), 2.5 (■), 3 (×), 4 (✧), and 5.2 K (▲) (χ'' is multiplied by a factor of 10).

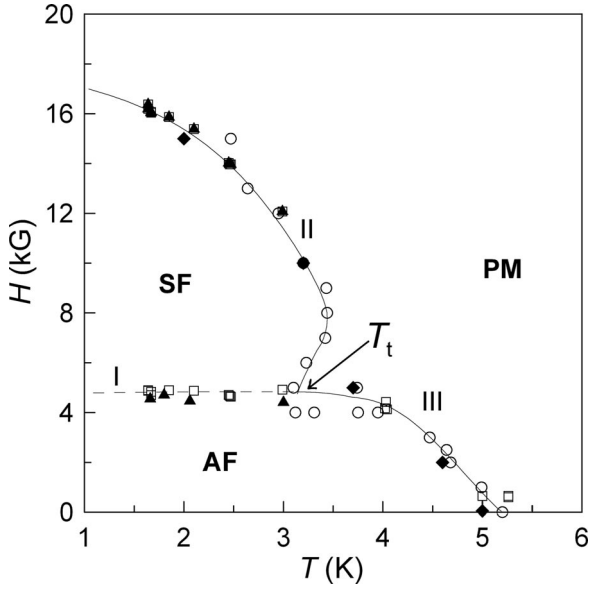

Figure 12. Phase diagram of compound **6**: $M(T)$ (♦), $M(H)$ (▲), $\chi'(T)$ (○), $\chi'(H)$ (□); T_t is the triple point; I denotes the first-order SF transition, and II and III denote second-order transitions (SF–PM and AF–PM phase boundaries).

To the best of our knowledge, compound **6** is the first decamethylmetallocenium-based CT salt, where an SF phase is detected, and thus contributes to the enrichment of the diversified magnetic behavior observed in this class of compounds.

Although no magnetic ordering was observed in compound **5** down to 1.6 K, this compound is expected to exhibit a similar behavior as that reported for **6** because of the absence of magnetic anisotropy of the donor. It is worth mentioning that a clear increase in $\chi'(T)$ is observed at low temperatures ($T < 5$ K), which suggests the onset of a 3D magnetic ordering.

In case of the $[Cr(Cp^*)_2]^+$-based CT salts, MM-like behavior was reported in the literature in the four compounds.[2a,24] However, no detailed analysis of their low-temperature magnetic behavior has been presented. Although they were reported as metamagnets, most probably, because of the absence of magnetic anisotropy of the donor, these salts must behave as Class II antiferromagnets and exhibit an SF phase, as observed in compound **6**. It is important to note that in $[Cr(Cp^*)_2]$DEtDCF,[24a] the behavior of the $M(T)$ curve strongly resembles that of **6** in the SF phase, which is clearly distinct from the behavior in the AF phase.

Conclusions

The crystal structures were correlated with the magnetic behavior of the CT salts of the series $[M(Cp^*)_2][M'(tds)_2]$, M/M′ = Fe/Ni (**1**), Fe/Pt (**2**), Mn/Ni (**3**), Mn/Pt (**4**), Cr/Ni (**5**), and Cr/Pt (**6**). These compounds show similar supramolecular arrangements and they are good examples of quasi-one-dimensional systems, since their crystal structures are based on a parallel arrangement of mixed chains, with short D–A intrachain separations and relatively large interchain separations. Compounds **1**–**5** are isostructural, and the CT salt **6** presents minor differences in the interchain arrangements.

The analysis of the intermolecular contacts in the structures of these compounds, in the framework of the McConnell I model, provides a reasonable interpretation of the intrachain and interchain magnetic coupling, and its relative value within this series of compounds. The magnetic behavior of these CT salts is dominated by FM interactions, which are assigned to strong FM D–A intrachain interactions. These interactions are attributed to the short contacts between the C atoms (with a negative ρ^S) from the Cp fragment of the donor and the metal and Se atoms (with a positive ρ^S) from the $M'Se_4$ core of the acceptor. The coexisting AF interchain interactions are attributed to the Se–Se contacts between acceptors in neighboring chains. In spite of being considerably weaker than the FM intrachain interactions, the AF interactions play a crucial role in the AF ordering detected in compounds **2**, **3**, **4**, and **6** (at low applied magnetic fields), with T_N = 3.3, 2.1, 5.8, and 5.2 K, respectively. A good relationship was observed between the spin of the donors (S_D) and the mean-field model predictions of the intrachain magnetic coupling and the ordering temperatures for the CT salts based on the $[M(Cp^*)_2]^+$ (M = Fe, Mn) donors (**1**, **2**, **3** and **4**). Compounds **5** and **6**, based on the $[Cr(Cp^*)_2]^+$ donor, display weaker intrachain coupling and lower critical temperatures than those predicted by that model, which is attributed to weaker D–A intrachain interactions.

The effect of the magnetic anisotropy of the donors is revealed in the field-induced transitions at low temperatures

 © 2008 Wiley-VCH Verlag GmbH & Co. KGaA, Weinheim

of CT salts **2**, **3**, **4**, and **6**. The CT salts based on the highly magnetic anisotropic donors $[M(Cp^*)_2]^+$ (M = Fe, Mn) are metamagnets (Class I antiferromagnets), and their phase diagrams include only two phases, an AF (low temperatures and low fields) and a PM phase (high temperatures and high fields). In the case of **6**, where the donor $[Cr(Cp^*)_2]^+$ does not exhibit any magnetic anisotropy, a more complex phase diagram was obtained. Besides the AF and PM phases, an SF phase was detected at low temperatures and intermediate magnetic fields (Class II antiferromagnet). Compound **6** is the first decamethylmetallocenium-based CT salt exhibiting an SF phase.

In the MM compounds, a good correlation was observed between the interchain AF coupling and the critical field, H_c. CT salts **2** and **4** are expected to display similar interchain AF coupling, and they exhibit H_c values of the same order. Compound **3**, in which the interchain coupling is expected to be considerably weaker, displays a lower H_c value.

No AF transitions were detected for compounds **1** and **5**, but they are expected to exhibit similar magnetic behavior at lower temperatures. Since they show weaker intra- and interchain magnetic coupling than their $[Pt(tds)_2]^-$-based analogue salts **2** and **6**, they are expected to behave as a Class I antiferromagnet (**1**) and a Class II antiferromagnet (**5**).

Experimental Section

General Remarks: Solvents were dried and distilled under nitrogen according to standard literature procedures,[25] acetonitrile and acetone were distilled under nitrogen over P_2O_5, and methanol and isobutyl alcohol were distilled under nitrogen from the corresponding magnesium alkoxides. The solvents were deaerated either by successive alternated freezing and evacuating cycles or by bubbling argon for approximately half an hour. $[Mn(Cp^*)_2]PF_6$[13d] and $[Cr(Cp^*)_2]PF_6$[14] were obtained from decamethylmanganocene (Strem Chemicals) and decamethylchromocene (Strem Chemicals), respectively, following previously described methods. The nBu$_4$N$[M(tds)_2]$ (M = Ni, Pt) salts were prepared by published literature procedures.[26] All syntheses and manipulations were carried out under nitrogen or argon, in a glovebox, or by using Schlenk techniques. Elemental analyses were carried out in a Carlo Erba (EA 1110-CHNS-O).

$[Mn(Cp^*)_2][Ni(tds)_2]$ (3): Decamethylmanganocenium bis[bis(trifluoromethyl)ethylene diselenolato] nickelate(III) was synthesized by the addition of a solution of $[Mn(Cp^*)_2]PF_6$ (50 mg, 0.106 mmol) in acetonitrile (10 mL) to a solution of nBu$_4$N$[Ni(tds)_2]$ (100 mg, 0.106 mmol) in methanol (14 mL), with constant stirring. After concentration for 2 h, a dark-green polycrystalline precipitate was collected by vacuum filtration. Yield: 77.2% (84 mg, 0.082 mmol). $C_{28}H_{30}F_{12}MnNiSe_4$ (1024.0): calcd. C 32.84, H 2.95,; found C 32.52, H 1.91%. Crystallization by slow evaporation of an acetone/isobutyl alcohol (4:1) concentrated solution of **3** afforded crystals suitable for X-ray diffraction.

$[Mn(Cp^*)_2][Pt(tds)_2]$ (4): Decamethylmanganocenium bis[bis(trifluoromethyl)ethylene diselenolato] platinate(III) was obtained by mixing a solution of $[Mn(Cp^*)_2]PF_6$ (50 mg, 0.106 mmol) in acetonitrile (10 mL) and a solution of nBu$_4$N$[Pt(tds)_2]$ (114 mg, 0.106 mmol) in methanol (12 mL). After concentration for 2 h, a dark polycrystalline precipitate was collected by vacuum filtration. Yield: 62.3% (77 mg, 0.066 mmol). $C_{28}H_{30}F_{12}MnPtSe_4$ (1160.4): calcd. C 28.98, H 2.61; found C 29.23, H 1.85%. Dark-green platelike crystals suitable for X-ray analysis were obtained by slow evaporation of an acetone-concentrated solution of **4** under inert atmosphere.

$[Cr(Cp^*)_2][Ni(tds)_2]$ (5): Decamethylchromocenium bis[bis(trifluoromethyl)ethylene diselenolato] nickelate(III) was obtained through slow addition of a solution of $[Cr(Cp^*)_2]PF_6$ (50 mg, 0.107 mmol) in acetonitrile (9 mL) to a solution of nBu$_4$N$[Ni(tds)_2]$ (101 mg, 0.107 mmol) in methanol (14 mL), with constant stirring. After concentration for 2 h, a dark-green polycrystalline precipitate was collected by vacuum filtration. Yield: 67.8% (74 mg, 0.073 mmol). $C_{28}H_{30}CrF_{12}NiSe_4$ (1021.1): calcd. C 32.94, H 2.96; found C 32.51, H 2.50%. Crystallization by slow evaporation of a dichloromethane/acetonitrile (1:1) concentrated solution of **5** afforded crystals suitable for X-ray diffraction.

$[Cr(Cp^*)_2][Pt(tds)_2]$ (6): Decamethylchromocenium bis[bis(trifluoromethyl)ethylene diselenolato] platinate (III) was synthesized by the addition of a solution of $[Cr(Cp^*)_2]PF_6$ (50 mg, 0.107 mmol) in acetonitrile (9 mL) to a solution of nBu$_4$N$[Pt(tds)_2]$ (115 mg, 0.107 mmol) in methanol (12 mL), with constant stirring. After concentration for 2 h, a dark-green polycrystalline precipitate was collected by vacuum filtration. Yield: 68% (84 mg, 0.073 mmol). $C_{28}H_{30}CrF_{12}PtSe_4$ (1157.5): calcd. C 29.06, H 2.61; found C 29.39, H 2.52%. It was possible to obtain dark-greenish platelike crystals suitable for X-ray analysis by slow evaporation of acetone-saturated solutions under inert atmosphere.

X-ray Crystallography

X-ray diffraction experiments for single crystals were performed with a Enraf Nonius CAD4 diffractometer by using graphite monochromated Mo-K_α radiation (λ = 0.71073 Å) in the ω-2θ scan mode. The relevant crystal, data collection, and refinement parameters are presented in Table 3. Unit-cell parameters were determined from the setting angles of 25 centered reflections. Orientation and intensity standard reflections were monitored, and no decay was detected. Data were corrected for Lorentz and polarization effects. Absorption was corrected semi-empirically by using the ψ-scan mode. The structures were solved by direct methods and refined by full-matrix least-squares with SHELXS-97[27] and SHELXL-97[28] by using the winGX software package.[29] Non-hydrogen atoms were refined anisotropically. In all the compounds, the CF_3 terminal groups show disorder, which were modeled over two positions, with the following occupation factors for each of the two CF_3 groups: 58:42% and 57:43%, 59:41% and 61:39%, 54:46% and 72:28%, and 68:32% and 60:40% for compounds **3**, **4**, **5**, and **6**, respectively. H atoms were placed in idealized positions and allowed to refine whilst riding on the parent C atom. The final difference Fourier map revealed the existence of residual electron densities of 3.1/–2.5 e A^{-3} for compound **4** and 1.71/–1.75 e A^{-3} for compound **6**. In both cases, the residual electron densities are located near the Pt atom. A summary of the crystal data, structure solution, and refinement is listed in Table 1. CCDC-684687, -684688, -684689, -684690 contain the supplementary crystallographic data for **3**, **4**, **5** and **6**, respectively. These data can be obtained free of charge from The Cambridge Crystallographic Data Centre via www.ccdc.cam.ac.uk/data_request/cif.

Magnetic Measurements

Static magnetic susceptibility data of polycrystalline samples of **3**–**6**, with the use of Teflon sample holders, were obtained with an

 © 2008 Wiley-VCH Verlag GmbH & Co. KGaA, Weinheim

Table 3. Crystallographic data for compounds **3**–**6**.

	[Mn(Cp*)$_2$][Ni(tds)$_2$] (**3**)	[Mn(Cp*)$_2$][Pt(tds)$_2$] (**4**)	[Cr(Cp*)$_2$][Ni(tds)$_2$] (**5**)	[Cr(Cp*)$_2$][Pt(tds)$_2$](**6**)
Formula	$C_{28}H_{30}F_{12}MnNiSe_4$	$C_{28}H_{30}F_{12}MnPtSe_4$	$C_{28}H_{30}F_{12}CrNiSe_4$	$C_{28}H_{30}F_{12}CrPtSe_4$
Formula weight	1024.0	1160.4	1021.1	1157.5
Temperature (K)	295(2)	295(2)	295(2)	295(2)
Crystal system, space group	triclinic, $P\bar{1}$	triclinic, $P\bar{1}$	ticlinic, $P\bar{1}$	mnoclinic, $C2/c$
a (Å)	8.5820(10)	8.6142(18)	8.580(3)	11.352(2)
b (Å)	10.471(5)	10.559(3)	10.541(4)	21.848(3)
c (Å)	11.1795(10)	11.221(2)	11.319(2)	14.969(2)
α (°)	108.40(5)	109.441(16)	109.51(2)	90
β (°)	103.57(2)	102.696(16)	103.21(2)	103.730(5)
γ (°)	101.79(5)	101.355(18)	101.72(4)	90
Volume (Å^3)	883.4(4)	897.5(4)	894.8(5)	3606.5(9)
Z, $D_{calcd.}$ (Mg m^{-3})	1, 1.925	1, 2.147	1, 1.895	4, 2.132
μ (mm^{-1})	5.093	8.381	4.979	8.294
F(000)	495	545	494	2176
Crystal size (mm)	0.06 × 0.04 × 0.03	0.035 × 0.019 × 0.016	0.06 × 0.02 × 0.02	0.058 × 0.018 × 0.014
θ Range (°)	2.56 to 25.02	2.71 to 25.02	2.56 to 25.03	2.73 to 25.02
Index range (h, k, l)	–10/9, –12/11, 0/13	–6/10, –12/12, –13/13	–10/0, –12/12, –13/13	–13/0, –26/0, –17/17
Reflections collected	3264	3557	3310	3310
Unique reflections [R_{int}]	3095 [0.0528]	3117 [0.0393]	3089 [0.0460]	3143 [0.0705]
Refined parameters	212	212	272	210
Goodness-of-fit	0.912	0.994	0.973	0.892
R_1 [$I > 2\sigma(I)$], wR_2	0.0769, 0.1120	0.0637, 0.1560	0.0555, 0.0824	0.0915, 0.1560
$\Delta\rho_{max,\ min}$ (e Å^{-3})	0.539, –0.579	3.169, –2.503	0.404, –0.344	1.711, –1.755

Oxford Instruments Faraday system, between 1.7 and 300 K, with a 70 kG superconducting magnet. Low temperature ($1.8 < T < 20$ K) dc magnetization data of polycrystalline samples in gelatine capsules were obtained with a Quantum Design SQUID (MPS) magnetometer, with a 55 kG superconducting magnet for compound **3** and with an Oxford Instruments Magnetometer (MagLab System 2000), with a 120 kG superconducting magnet, by using the extraction method ($T > 1.6$ K) for CT salts **4**, **5**, and **6**. The ac susceptibility measurements with polycrystalline samples of **4**–**6** were also obtained with the MagLab system, with an ac field of 1 G. Susceptibility and magnetization data were corrected for contributions arising from sample holder and core diamagnetism, which were estimated from tabulated Pascal constants.

Supporting Information (see footnote on the first page of this article): Detailed descriptions of the intrachain and interchain arrangements of the CT salts **1**–**6** are shown.

Acknowledgments

This work was partially supported by Fundação para a Ciência e Tecnologia (Portugal) under contract PTDC/QUI/65379/2006. This work also benefited from COST action D35 and the MAGMANet network of excellence.

[1] a) H. M. McConnell, *J. Chem. Phys.* **1963**, *39*, 1910; b) H. M. McConnell, *Proc. Robert A Welch Found. Conf. Chem. Res.* **1967**, *11*, 144.

[2] a) G. T. Yee, J. S. Miller, *Magnetism: Molecules to Materials V* (Eds: J. S. Miller, M. Drillon), Wiley-VCH, Weinheim, Germany, **2005**, pp. 223–260; b) V. Gama, M. T. Duarte, *Magnetism: Molecules to Materials V* (Eds: J. S. Miller, M. Drillon), Wiley-VCH, Weinheim, Germany, **2005**, pp. 1–40.

[3] J. S. Miller, J. C. Calabrese, H. Rommelmann, S. R. Chittipeddi, J. H. Zhang, W. M. Reiff, A. J. Epstein, *J. Am. Chem. Soc.* **1987**, *109*, 769–781.

[4] C. Kollmar, M. Couty, O. Kahn, *J. Am. Chem. Soc.* **1991**, *113*, 7994–8005.

[5] H. Heise, F. H. Köhler, M. Herker, W. Hiller, *J. Am. Chem. Soc.* **2002**, *124*, 10823–10832.

[6] J. Schweizer, A. Bencini, C. Carbonera, A. J. Epstein, S. Golhen, E. Lelièvre-Berna, J. S. Miller, L. Ouahab, Y. Pontillon, E. Ressouche, A. Zheludev, *Polyhedron* **2001**, *20*, 1771–1778.

[7] For a general review on metal–bis(dithiolene)-based materials see: N. Robertson, L. Cronin, *Coord. Chem. Rev.* **2002**, *227*, 93–127.

[8] S. Rabaça, R. Meira, L. C. J. Pereira, M. T. Duarte, J. J. Novoa, V. Gama, *Inorg. Chim. Acta* **2001**, *326*, 89–100.

[9] V. Gama, D. Belo, S. Rabaça, I. C. Santos, H. Alves, J. C. Waerenborgh, M. T. Duarte, R. T. Henriques, *Eur. J. Inorg. Chem.* **2000**, 2101–2110.

[10] J. S. Miller, J. C. Calabrese, A. J. Epstein, *Inorg. Chem.* **1989**, *28*, 4230–4238.

[11] J. S. Miller, A. J. Epstein, *Research Frontiers in Magnetochemistry* (Ed.: C. J. O′′onnor), World Science Singapore, **1993**, pp. 283–302.

[12] Preliminary results of this compound were presented in V. Gama, S. Rabaça, C. Ramos, D. Belo, I. C. Santos, M. T. Duarte, *Mol. Cryst. Liq. Cryst.* **1999**, *335*, 81–90.

[13] a) B. B. Kaul, W. S. Durfee, G. T. Yee, *J. Am. Chem. Soc.* **1999**, *121*, 6862–6866; b) W. E. Broderick, J. A. Thompson, E. P. Day, B. M. Hoffman, *Science* **1990**, *249*, 401–403; c) J. S. Miller, R. S. McLean, C. Vazquez, G. T. Yee, K. S. Narayan, A. J. Epstein, *J. Mater. Chem.* **1991**, *1*, 479–480; d) J. L. Robbins, N. M. Edelstein, S. R. Cooper, J. C. Smart, *J. Am. Chem. Soc.* **1979**, *101*, 3853–3857; e) C. Faulmann, E. Rivière, S. Dorbes, F. Senocq, E. Coronado, P. Cassoux, *Eur. J. Inorg. Chem.* **2003**, 2880–2888; f) W. E. Broderick, J. A. Thompson, B. M. Hoffman, *Inorg. Chem.* **1991**, *30*, 2958–2960.

[14] J. L. Robbins, N. M. Edelstein, B. Spencer, J. C. Smart, *J. Am. Chem. Soc.* **1982**, *104*, 1882–1893.

[15] W. B. Heuer, A. E. True, P. N. Swepston, B. M. Hoffman, *Inorg. Chem.* **1988**, *27*, 1474–1482.

[16] E. Keller, *SCHAKAL-97*, *A Computer Program for the Representation of Molecular and Crystallographic Models*, Kristallographisches Institut der Universität Freiburg i. Br., Germany, **1997**.

 © 2008 Wiley-VCH Verlag GmbH & Co. KGaA, Weinheim

[17] J. S. Miller, A. J. Epstein, *Angew. Chem. Int. Ed. Engl.* **1994**, *33*, 385–415 and references therein.
[18] a) J. Blumel, N. Hebendaz, P. Hudeczek, F. H. Kohler, W. Strauss, *J. Am. Chem. Soc.* **1992**, *114*, 4223–4230; b) C. Kollmar, O. Kahn, *J. Chem. Phys.* **1992**, *96*, 2988–2997; c) H. Heise, F. H. Köhler, M. Herker, W. Hiller, *J. Am. Chem. Soc.* **2002**, *124*, 10823–10832.
[19] J. Scweitzer, A. Bencini, C. Carbonera, A. J. Epstein, S. Golhen, E. Lelièvre-Berna, J. S. Miller, L. Ouahab, Y. Pontillon, E. Ressouche, A. Zheludev, *Polyhedron* **2001**, *20*, 1771–1778.
[20] E. Stryjewski, N. Giordano, *Adv. Phys.* **1977**, *26*, 487–650.
[21] H. A. Groenendijk, A. J. van Duyneveldt, *Physica* **1982**, *115B*, 41–62.
[22] A. Narath, *Phys. Rev.* **1965**, *139*, A1221–A1227.
[23] a) H. Ehrenberg, B. Schwarz, H. Weitzel, *J. Magn. Magn. Mater.* **2006**, *305*, 57–62; b) M. Morocoima, M. Quintero, E. Quintero, J. González, R. Tovar, P. Bocaranda, J. Ruiz, N. Marchán, D. Caldera, E. Calderon, J. C. Woolley, G. Lamarche, A.-M. Lamarche, J. M. Broto, H. Rakoto, L. D′Onofrio, R. Cadenas, *J. Appl. Phys.* **2006**, *100*, 053907; c) R. Cadenas, M. Quintero, E. Quintero, R. Tovar, M. Morocoima, J. González, J. Ruiz, J. M. Broto, H. Rakoto, J. C. Woolley, G. Lamarche, *Physica B* **2004**, 346–347.
[24] a) B. B. Kaul, R. D. Sommer, B. C. Noll, G. T. Yee, *J. Solid State Chem.* **2001**, *159*, 420–427; b) W. S. Tyree, C. Slebonick, M. C. Spencer, G. Wang, J. S. Merola, G. T. Yee, *Polyhedron* **2005**, *24*, 2133–2140.
[25] D. D. Perrin, W. L. F. Armarego, *Purification of Laboratory Chemicals*, Pergamon Press, Oxford, **1988**.
[26] a) W. B. Heuer, A. E. True, P. N. Swepston, B. M. Hoffman, *Inorg. Chem.* **1988**, *27*, 1474–1482; b) J. Morgado, Ph. D. Thesis, Universidade Técnica de Lisboa, Instituto Superior Técnico, **1995**; c) S. Rabaça, Ph. D. Thesis, Universidade Técnica de Lisboa, Instituto Superior Técnico, **2004**.
[27] G. M. Sheldrick, *SHELXS-97, A Program for Crystal Structure Determination*, University of Göttingen, Göttingen, Germany, **1990**; G. M. Sheldrick, *Acta Crystallogr., Sect. A* **1990**, *46*, 467 for direct methods SHELXS-97.
[28] G. M. Sheldrick, *SHELXL97*, *Program for Crystal Structure Refinement*, University of Göttingen, Germany, **1997**.
[29] L. J. Farrugia, *J. Appl. Crystallogr.* **1999**, *32*, 837–837.

Received: April 15, 2008
Published Online: July 10, 2008

 © 2008 Wiley-VCH Verlag GmbH & Co. KGaA, Weinheim